Generation mechanisms of fundamental rogue wave spatial-temporal structure

Liming Ling,[1,*] Li-Chen Zhao,[2,3,*] Zhan-Ying Yang,[2,3] and Boling Guo[4]
[1]*School of Mathematics, South China University of Technology, Guangzhou 510640, China*
[2]*School of Physics, Northwest University, Xi'an 710069, China*
[3]*Shaanxi Key Laboratory for Theoretical Physics Frontiers, Xi'an 710069, China*
[4]*Institute of Applied Physics and Computational Mathematics, Beijing 100088, China*
(Received 6 November 2016; revised manuscript received 1 March 2017; published 22 August 2017)

We discuss the generation mechanism of fundamental rogue wave structures in N-component coupled systems, based on analytical solutions of the nonlinear Schrödinger equation and modulational instability analysis. Our analysis discloses that the pattern of a fundamental rogue wave is determined by the evolution energy and growth rate of the resonant perturbation that is responsible for forming the rogue wave. This finding allows one to predict the rogue wave pattern without the need to solve the N-component coupled nonlinear Schrödinger equation. Furthermore, our results show that N-component coupled nonlinear Schrödinger systems may possess N different fundamental rogue wave patterns at most. These results can be extended to evaluate the type and number of fundamental rogue wave structure in other coupled nonlinear systems.

DOI: 10.1103/PhysRevE.96.022211

I. INTRODUCTION

Rogue waves (RWs), including scalar and vector ones, have been observed in many different physical systems [1–6]. The RWs have some different fundamental spatial-temporal structures, such as an eye-shaped one, an anti-eye-shaped one, and a four-petaled one. Scalar RWs usually admit the eye-shaped one [7–10], while vector RWs can admit anti-eye-shaped and four-petaled ones [11–17]. The nonlinear superposition of these fundamental RWs corresponds to high-order RWs or multiple RWs, which could admit much more complex structures [18–23]. Therefore, the understanding of the fundamental RWs is the first step to explain the complex dynamics of RWs. Present studies have shown that RWs arise from modulational instability (MI) which is associated with the growth of perturbations on a plane wave background [24]. Furthermore, it is found that baseband MI or MI with resonant perturbations plays an essential role in RW excitations [25–27], and much effort has been given to the general nature of the nonlinear stage of MI to understand MI more systematically [28,29]. However, the underlying mechanisms to form different spatial-temporal structures of fundamental RWs have not been clear.

Previous studies of RWs were mainly focused on low-component systems such as one-, two-, or three-component systems [8,11–15]. However, in real physical systems, there are many coupled systems which have high components, such as five-component (spin-2 spinor Bose-Einstein condensate [30]) or seven-component (spin-3 spinor Bose-Einstein condensate [31]) ones, and multimode fiber [32]. In comparison with low-component systems, the dynamical behaviors and relevant patterns of RWs of high-component systems are less studied, partly because of the difficulties in solving N-component coupled nonlinear equations.

In this paper, we discuss the mechanism of fundamental RW structures in N-component coupled systems through analyzing an analytical solution of nonlinear Schrödinger equations and the related MI dispersion form. We show that the evolution energy and growth rate of resonant perturbations on a plane wave background play a dominant role in shaping the basic patterns of RWs. Due to this mechanism, the N-component coupled systems can possess N different fundamental patterns at most. Based on these findings and MI analysis, we propose a simple method to predict the structures and numbers of fundamental RWs of a nonlinear system.

II. THE COUPLED NONLINEAR SCHRÖDINGER EQUATION WITH ARBITRARY COMPONENT NUMBER

Among the models for RW excitations, the nonlinear Schrödinger equation (NLSE) is one of the most representative models for its wide applications in many different physical systems [1], and many RW experiments have suggested that the rational solutions of the NLSE indeed describe RW phenomena well [2–6]. Therefore, we consider the following focusing vector NLSE with arbitrary component number N [33,34]:

$$i\mathbf{q}_t + \tfrac{1}{2}\mathbf{q}_{xx} + \mathbf{q}\mathbf{q}^{\dagger}\mathbf{q} = 0, \tag{1}$$

where $\mathbf{q} = (q_1, q_2, \ldots, q_N)^T$, and T and $\dagger$ represent the transpose and the Hermite conjugation of a matrix, respectively. The vector NLSE can be used to describe the evolution of localized waves in a nonlinear fiber with multimodes [35], multicomponent Bose-Einstein condensate [36–38], and other nonlinear coupled systems [1]. The model can be used to conveniently discuss both scalar NLSE with $N = 1$ and vector NLSE with $N > 1$, which enables us to discuss general properties for a RW. It has been shown that there are mainly three RW fundamental structures, such as eye-shaped, anti-eye-shaped, and four-petaled ones in two- or three-component cases [12,14,33,39].

III. THE MECHANISM FOR ROGUE WAVE SPATIAL-TEMPORAL STRUCTURE

To understand the mechanism of fundamental RW structures, it is meaningful to derive a simple form to describe

*Corresponding authors: zhaolichen3@nwu.edu.cn; linglm@scut.edu.cn

their dynamics. The general form for a fundamental RW with N components can be followed with the method provided in [40]. The fundamental RW solution for the above vector NLSE with arbitrary component number can be presented as

$$q_i = a_i\left\{1+\frac{2i(\chi_R+b_i)(x+\chi_R t)-2i\chi_I^2 t-1}{A_i\left[(x+\chi_R t)^2+\chi_I^2 t^2+\frac{1}{4\chi_I^2}\right]}\right\}e^{\theta_i}, \quad (2)$$

where $A_i=(\chi_R+b_i)^2+\chi_I^2$, $\theta_i=i[b_i x+(|a|^2-\frac{1}{2}b_i^2)t]$ ($|a|^2=\sum_{i=1}^N a_i^2$), $i=1,2,\ldots,N$, a_i and b_i are the amplitude and wave vector of the background in component i, respectively, $\chi_R=\mathrm{Re}(\chi)$, and $\chi_I=\mathrm{Im}(\chi)$. χ is a root for the following equation:

$$1+\sum_{i=1}^{N}\frac{a_i^2}{(\chi+b_i)^2}=0, \quad (3)$$

with $\mathrm{Im}(\chi)>0$. It is easy to see that the above equation possesses N pairs of conjugated complex roots provided that there are N different b_i's and nonzero a_i's. Through analyzing the extreme points of the RW solution on a spatial-temporal distribution plane, we find that the value of $\frac{(\chi_R+b_i)^2}{\chi_I^2}$ can be used to conveniently make a judgment regarding the RW pattern in NLSE described systems. If $\frac{(\chi_R+b_i)^2}{\chi_I^2}\leqslant\frac{1}{3}$, then a fundamental RW possesses the well-known eye-shaped structure on spatial-temporal distribution; if $\frac{(\chi_R+b_i)^2}{\chi_I^2}\geqslant 3$, then the RW possesses an anti-eye-shaped structure; if $\frac{1}{3}<\frac{(\chi_R+b_i)^2}{\chi_I^2}<3$, then the RW admits a four-petaled structure. Each structure of fundamental RW can be varied with the value changing of $\frac{(\chi_R+b_i)^2}{\chi_I^2}$. This enables one to analyze the RW pattern based on a related solution, but the underlying mechanism for forming different RW patterns is still obscure.

Previous studies have suggested that MI can be used to understand RW excitation [25,27]. A spectrum analyzing method was developed to distinguish RW and breathers generated from a turbulence [41]. However, the relations between the MI and RW pattern are still obscure. But these results provide some hints to solve the above problem. We revisit the standard MI analysis and obtain a simple form for the MI dispersion relation [25]. This enables us to obtain quantitative relations between the RW pattern and MI characters. Linear stability analysis is performed on N-component plane wave backgrounds,

$$q_i[0]=a_i\exp\theta_i. \quad (4)$$

The linearized stability of perturbations on the plane wave solution can be obtained by adding weak perturbations with Fourier modes. We perturb the seed solution in the following way:

$$q_i=q_i[0][1+p_i(x,t)].$$

Keeping the linear terms of $p_i(x,t)$, the linearized disturbance equations become

$$i(p_{i,t}+b_i p_{i,x})+\frac{1}{2}p_{i,xx}+\sum_{l=1}^{N}(p_l+p_l^*)=0, \quad (5)$$

$i=1,2,\ldots,N$, where superscript * represents the complex conjugate. The perturbations $p_i(x,t)$ are periodical in x with the period $2L$, $-L<x\leqslant L$. Thus, p_i has the Fourier expansion

$$p_i(x,t)=\frac{1}{2L}\sum_{k=-\infty}^{+\infty}\widehat{p_{i,k}}e^{i\mu_k x},$$

where $\mu_k=2\pi k/2L$, $\widehat{p_{i,k}}=\int_{-L}^{L}p_i(x,t)e^{i\mu_k x}dx$. Since the partial differential equation (PDE) is linear, it is sufficient to consider

$$p_i(x,t)=\widehat{p_{i,-k}}e^{-i\mu_k x}+\widehat{p_{i,k}}e^{i\mu_k x} \quad (6)$$

for $k\neq 0$, while for $k=0$,

$$p_i(x,t)=\widehat{p_{i,0}(t)}.$$

With the above analysis, we can obtain the MI analysis for the periodical perturbation. We give the judging criteria for $k\neq 0$. Based on the above Eqs. (5) and (6), we can set

$$\widehat{p_{i,k}}=e^{i\mu_k\Omega_k t}p_{i,k},\quad \widehat{p_{i,-k}}=e^{-i\mu_k\Omega_k^* t}p_{i,-k}^*,$$

where Ω_k is a complex number. Then we obtain the following equation:

$$KY=0, \quad (7)$$

where

$$\begin{aligned}K=\mathrm{diag}\big[&\left(-\Omega_k-b_1-\tfrac{1}{2}\mu_k\right)\mu_k,\left(-\Omega_k+b_1-\tfrac{1}{2}\mu_k\right)\mu_k,\\&\ldots,\left(-\Omega_k-b_N-\tfrac{1}{2}\mu_k\right)\mu_k,\\&\left(-\Omega_k+b_N-\tfrac{1}{2}\mu_k\right)\mu_k\big]+H\left(a_1^2,a_1^2,\ldots,a_N^2,a_N^2\right),\end{aligned}$$

$$H=(1,1,\ldots,1,1)^{\mathrm{T}},\quad Y=\left(p_{1,k},p_{1,-k},\ldots,p_{N,k},p_{N,-k}\right)^{\mathrm{T}}.$$

The determinant of matrix K is

$$\begin{aligned}\det(K)=\mu_k^{2N}\sum_{l=1}^{N}\left[\frac{1}{4}\mu_k^2-(\Omega_k+b_l)^2\right]^2\\\times\left[1+\sum_{l=1}^{N}\frac{a_l^2}{(\Omega_k+b_l)^2-\frac{1}{4}\mu_k^2}\right].\end{aligned}$$

To let the vector Y have nonzero solution, the determinant $\det(K)$ must be equal to zero, which is the dispersion relation for linearized disturbance:

$$1+\sum_{l=1}^{N}\frac{a_l^2}{(\Omega_k+b_l)^2-\frac{1}{4}\mu_k^2}=0. \quad (8)$$

For $k=0$, we then obtain

$$\frac{d}{dt}\mathrm{Re}(\widehat{p_{i,0}})=0,$$

$$\frac{d}{dt}\mathrm{Im}(\widehat{p_{i,0}})=2\sum_{l=1}^{N}a_l^2\mathrm{Re}(\widehat{p_{i,0}}).$$

It is obvious that $\widehat{p_{i,0}}=\alpha_i+i\beta_i t$, where α_i and β_i are some undetermined real parameters. Thus we know that this perturbation is instable. The usual way to avoid this instability is choosing $\int_{-L}^{L}p_i(x,0)dx=0$.

In this work, to study the localized perturbation, we use the limit technique through taking limit $\mu_k\to 0$, i.e., $L\to\infty$. Then the above Fourier series becomes Fourier transformation.

However, to establish the relation with the RW solution, we still use the denotation of the Fourier series. We have shown that RW comes from the resonance perturbation in the MI regime [27]. Resonance perturbation also means that the limit of perturbation wave vector $\mu_k \to 0$ is taken to simplify the dispersion relation [42]. The final simplified dispersion relation is

$$1 + \sum_{i=1}^{N} \frac{a_i^2}{(\Omega_k + b_i)^2} = 0, \tag{9}$$

which agrees precisely with the equation of χ determining the fundamental RW pattern (3).

Im$[\Omega_k]$ denotes the growth rate of a perturbation and Re$[\Omega_k]$ denotes the evolution energy of the perturbation. One can see that the parameters χ and Ω_k satisfy an identical equation (3) or (9). The dispersion form for perturbations Ω_k can be used to know χ_R and χ_I directly for certain backgrounds, namely, $\chi = \Omega_k$. This is an equation correspondence, which is distinctive from the inequation correspondence for RW existence condition and baseband MI [25]. The value of $\frac{(\chi_R+b_i)^2}{\chi_I^2}$ can be used to conveniently make a judgment regarding the RW pattern in NLSE described systems. Obviously, if Im$[\Omega_k] = 0$, there will be no MI character, and the corresponding relation $\chi_I = 0$ makes the RW solution meaningless. This character agrees well with the MI mechanism for RW in previous studies [25,27]. In this way, the linear stability analysis on plane wave backgrounds provides us with direct information for the RW pattern.

This enables us to explain why the scalar NLSE always admits an eye-shaped pattern for a fundamental RW. For a scalar NLSE, there is only one component for which the background amplitude is denoted by a and the wave vector is denoted by b. Then the dispersion relation gives us the dispersion form $\Omega_k = -b + a\ i = \chi$. The $\frac{(\chi_R+b)^2}{\chi_I^2} = 0$ will always be smaller than $\frac{1}{3}$, which means that the fundamental RW for a scalar NLSE is always an eye-shaped one. Similar calculations can be used to explain why the anti-eye-shaped RW and four-petaled RW exist for vector RWs [14–17]. The previous studies indicated that a RW just exists in the cases with Im$[\Omega_k] \neq 0$. But the RW pattern must be observed numerically or experimentally. Here we report that the parameters Re$[\Omega_k]$ and Im$[\Omega_k]$ can provide the fundamental RW pattern type directly on certain backgrounds for NLSE described systems. Namely, the evolution energy value and growth rate of a resonant perturbation on a certain plane wave background determine the structure of a fundamental RW. The results allow one to predict the RW pattern and even the number of fundamental RWs from linear stability analysis on a plane wave background, without the need to solve the vector NLSE. This is the main result of this paper.

IV. PREDICT ROGUE WAVE PATTERN BASED ON DISPERSION FORMS

The quantitative relation between the RW and MI provides possibilities to predict the RW pattern based on the dispersion form of linear stability analysis. The above equation (3) possesses N pairs of conjugated complex roots, which means there are N different fundamental RW patterns. Each branch determines one fundamental structure. For an example, we show how to do this in a five-component case. We consider a case in which all five plane wave background amplitudes are $a_i = 1$, and the wave vectors are $b_1 = -2, b_2 = -1, b_3 = 0, b_4 = 1, b_5 = 2$. For these backgrounds, we can calculate the dispersion relation directly and obtain five branches of dispersion relations for Ω_k, namely, $\Omega_k(1) \approx 1.76 + 0.68i$, $\Omega_k(2) \approx 0.90 + 0.79i$, $\Omega_k(3) \approx 0.79i$, $\Omega_k(4) \approx -0.90 + 0.79i$, $\Omega_k(5) \approx -1.76 + 0.68i$. The real part and imaginary part of Ω_k can be used to make a judgment regarding the RW patterns by combing the general form for a fundamental RW. We can know that there are five patterns in this case. Each pattern can be known from the above classifying condition for the RW pattern. The results are shown in an arbitrary one-component case by the exact RW solutions (the following general multi-RW solution for a coupled NLSE with arbitrary N components). There are one eye-shaped, two anti-eye-shaped, and two four-petaled RWs in the third component for the five-component coupled case [Fig. 1(a)]. The results indicate that the dispersion form indeed could be used to predict the RW pattern. It should be pointed out that several RWs belonging to one type of fundamental RW pattern can still be distinctive from each other. This can be validated by direct analysis of them. A similar process can be done for many other cases [Fig. 1(b) for a six-component case]. A double RW and triple RW have been obtained in two-component and three-component coupled systems for several years [12,14,33], but the underlying reasons for them have not been explained. The results here can be used to explain them directly. Explicitly, the two or three RWs come from the two or three branches of the MI dispersion form. Next, we present a multi-RW solution of the vector NLSE with arbitrary N components, which can be used to conveniently observe the dynamics of fundamental RWs and their nonlinear superposition in NLSE described systems and support the above main results of this paper.

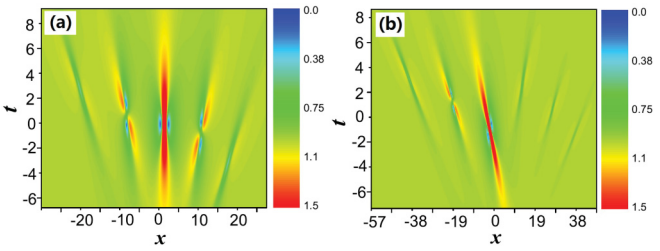

FIG. 1. The rogue wave patterns in the third component for (a) five-component case and (b) six-component coupled case. It is seen that there are two anti-eye-shaped rogue waves, two four-petaled ones, and one eye-shaped one in (a). There are four anti-eye-shaped ones, one eye-shaped one, and one four-petaled one in (b). The anti-eye-shaped rogue waves are a bit different from each other. The results agree precisely with the patterns predicted by modulational instability analysis. Parameters: (a) $a_i = 1, b_1 = -2, b_2 = -1, b_3 = 0, b_4 = 1, b_5 = 2, x_1 = -20, x_2 = -10, x_3 = 0, x_4 = 10, x_5 = 20, t_i = 0$, $(i = 1,2,3,4,5)$; (b) $a_i = 1$, $b_1 = -3, b_2 = -2, b_3 = -1, b_4 = 1, b_5 = 2, b_6 = 3, x_1 = -37.5$, $x_2 = -22.5, x_3 = -7.5, x_4 = 7.5, x_5 = 22.5, x_6 = 37.5, t_i = 0$ $(i = 1,2,3,4,5,6)$.

V. M-ROGUE WAVE FOR THE VECTOR NLSE

The soliton solution and even the multisoliton solution on a zero background of vector NLSE have been widely derived [43–45]. RWs on a nonzero background have been derived for up to $N = 3$ components. We give a general formula for fundamental RWs and their nonlinear superposition in the N-component case. To obtain general M-RW solutions for the vector NLSE, we choose a general plane wave solution (4). In this same way as for deriving a nonlinear wave solution through Darboux transformation [46,47], we obtain the following M-RW solution by the generalized Darboux transformation with the formal series technique proposed in [40]:

$$q_i = a_i \left[\frac{\det(F^{[i]})}{\det(F)}\right] e^{\theta_i}, \tag{10}$$

where

$$F = (F_{k,j})_{1\leqslant k,j\leqslant M}, \quad F^{[i]} = \left(F^{[i]}_{k,j}\right)_{1\leqslant k,j\leqslant M},$$

$$F_{k,j} = \frac{1}{\chi_k^* - \chi_j}\left[X_j X_k^* - \frac{i(X_j + X_k^*)}{\chi_k^* - \chi_j} - \frac{2}{(\chi_k^* - \chi_j)^2}\right],$$

$$F^{[i]}_{k,j} = \frac{1}{\chi_k^* - \chi_j}\left\{\left(iX_j - \frac{1}{\chi_j + b_i}\right)\left(-iX_k^* + \frac{1}{\chi_k^* + b_i}\right) + \frac{-i(X_j + X_k^*) + \frac{1}{\chi_k^* + b_i} + \frac{1}{\chi_j + b_i}}{\chi_k^* - \chi_j} - \frac{2}{(\chi_k^* - \chi_j)^2}\right\},$$

$M \leqslant N$, $X_j = x - x_j + \chi_j(t - t_j) - \frac{1}{2\mathrm{Re}(\chi_j)}$, x_j and t_j are real constants, and χ_j satisfies the equation

$$1 + \sum_{i=1}^{N} \frac{a_i^2}{(\chi_j + b_i)^2} = 0, \tag{11}$$

with $\mathrm{Im}(\chi_j) > 0$. It is easy to see that the above equation possesses N pairs of conjugated complex roots provided that there are N different b_i and nonzero a_i. The N pairs of conjugated complex roots correspond to N branches of MI dispersion forms. This means that N different RW patterns correspond to N branches of MI dispersion forms. It should be emphasized that the maximum number of fundamental RWs is N in the N-component case, and the number can be other integer values smaller than N for some degenerate cases. The M-RW is a multi-RW solution, which is a nonlinear superposition of different fundamental RWs. It is different from high-order RW solutions which are nonlinear iterations from an identical fundamental RW. With the high-order expansion for the related parameters, the general high-order RW solutions can be constructed exactly [48].

The numbers of vector RWs in a temporal-spatial distribution plane are different from the ones in scalar systems. We have demonstrated that two or four fundamental RWs can emerge on the distribution plane [12,39], in contrast to the nth-order RWs of scalar NLSE for which there are merely $n(n+1)/2$ eye-shaped ones or their superposition forms [18,19,21,49,50]. Then, how many different numbers can exist on a spatial-temporal distribution plane for vector RWs? Through the above RW solution, one can prove that there are N fundamental RWs for the N-component NLSE at most. For example, there are one eye-shaped, one four-petaled, and four anti-eye-shaped RWs in the third component for the six-component coupled case [Fig. 1(b)]. In particular, the six RWs here belong to a multi-RW, which is distinctive from the high-order RWs. The third-order RW for scalar NLSE also admits six RWs, but the six RWs always admit an eye-shaped one. Moreover, the six RWs here admit more freedom than the high-order scalar RWs; the location of each RW can be changed separately. Therefore, we call these types of RWs as multi-RWs to make them distinct from the high-order ones. The method can be used to generate high-order RWs. A general form for high-order RW solutions is presented in Ref. [48]. Since we mainly intend to explain the mechanism of the fundamental RW structure in this paper, the high-order RW solutions are not presented in detail.

VI. POSSIBILITIES TO TEST THE THEORETICAL RESULTS IN EXPERIMENTS

The MI analysis can be used to predict the RW pattern in an N-component coupled system, which is supported by exact solutions in the above discussions. However, a RW can also be observed from many different initial perturbation conditions. Recent studies indicate that the RW comes from MI with resonance perturbations or baseband MI [25–27]. It should be noted that there have been some important works that discuss the robust property against perturbation and nonlinear MI [29,51–53]. Very recently, the orbital stability and spectral stability for the classical RW solutions were discussed well in [54,55], respectively. These results further disclose and enrich the instability property for RWs. The RW pattern does not depend on the profile of initial perturbations and it is determined by the MI characters of the nonlinear systems. Therefore, eye-shaped RWs or breathers have been observed from many different initial conditions [24,56,57]. Then, we simulate the evolution numerically from the initial conditions given by the exact solution with parameter deviations in the $N = 3$ components case, to show that N fundamental RWs come from the N branches of MI dispersion forms. There are three branches of MI dispersion forms, which means there are three different patterns in this case. The pattern can be predicted by the linear MI dispersion form. Numerical simulations suggest that the RW patterns are robust against weak parameter derivations. As an example, we choose one branch of the MI dispersion form for which three fundamental RW patterns emerge in the three-component case separately. With $a_j = 1\,(j = 1,2,3)$, $b_1 = 1$, $b_2 = 0$, and $b_3 = -1$, an anti-eye-shaped RW emerges in the q_1 component, a four-petaled RW emerges in the q_2 component, and an eye-shaped RW emerges in the q_3 component. The numerical evolution from the ideal initial condition given by the exact solution (2) with $\chi = \chi_1 \equiv (1+i)\sqrt{2}/2$ at $t = -3$ is shown in the left column in Fig. 2. We exhibit the numeric evolution of the initial condition given by an exact one with parameter deviations $\chi = \chi_1 + \mathrm{rand}(1)/80$, where rand(1) is random complex numbers with norm less than 1, shown in the right column in Fig. 2 . It is shown that the RW patterns are indeed robust against parameter deviations.

Furthermore, we perform the numerical evolution of the ideal initial data with Gaussian white noises to test the robustness of RW signals. We use the awgn function with the

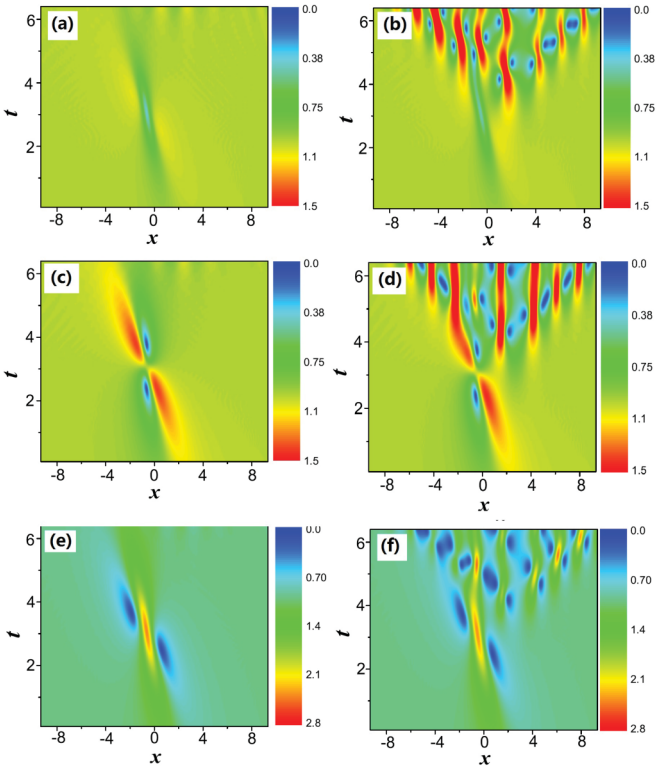

FIG. 2. The numerical stability test of the rogue wave against parameter deviations in a three-component case. The numerical evolution from the ideal initial condition given by the exact solution at $t = -3$ is shown in the left columns. The results with parameter deviation are shown in the right columns. The figures in the ith row represent the density plot of $|q_i|$ $(i = 1,2,3)$, (a), (b) $|q_1|$; (c), (d) $|q_2|$; (e), (f) $|q_3|$. It is shown that rogue waves are stable against parameter deviations.

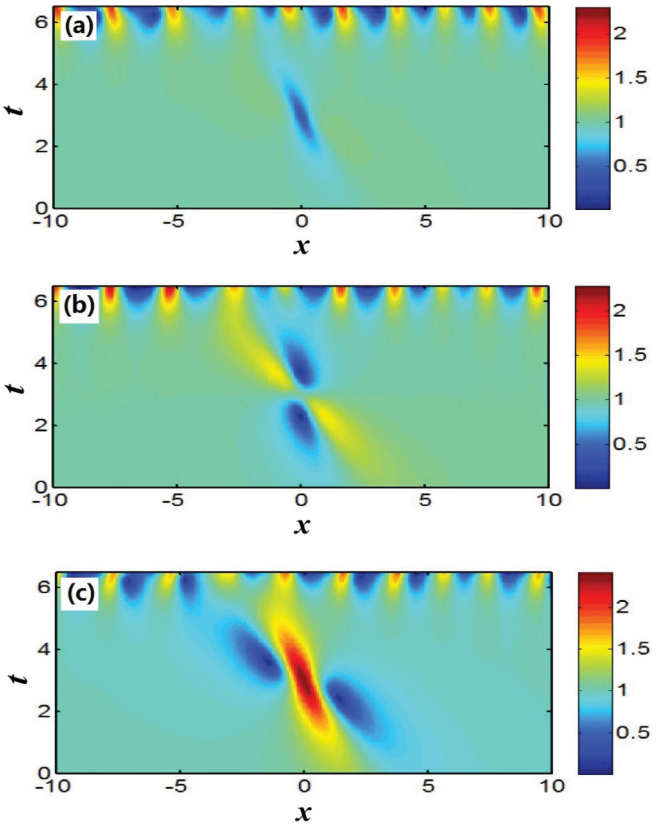

FIG. 3. The numerical evolution from the ideal initial condition with Gaussian white noises. The three figures represent the density plot for the three different components $(|q_1|,|q_2|,|q_3|)$ for the three-component NLSE. It is shown that the rogue wave signals are robust against the noises.

signal to noise ratio 100 using MATLAB to achieve the noise, and the initial data are given by the exact solution at $t = -3$ (as the ones in Fig. 2). As shown in Fig. 3, we see that the RWs are still robust against the weak noises. Additionally, the backgrounds admit MI, which makes the weak perturbations evolve to be large amplitude waves. This explains that the large amplitude periodical waves occur around the time $t = 6$. But this does not affect the spatial-temporal structure of RWs. That is to say, the exact RW solutions are useful for preparing the initial data in the experiments even with small deviations. Recently, a dark RW (anti-eye-shaped RW) was observed in a real experiment [5] and MI in a vector system was demonstrated in a Manakov fiber system [6]. The results here have great possibilities to be checked in nonlinear fibers with two or more modes.

VII. CONCLUSION

In summary, we show that the evolution energy and growth rate of resonant perturbations determine the RW pattern type on certain backgrounds for NLSE described systems. To understand the quantitative relation more clearly, we discuss the pattern formation of the Akhmediev breather (AB) since the RW solution is a limit of the AB solution.

The fundamental AB solution can be constructed by the Darboux transformation [46–48], which is represented as follows:

$$q_i = a_i \left(\frac{\frac{\chi^* + b_i}{\chi + b_i} e^{\omega_R} + \frac{\chi^* + b_i + \alpha}{\chi + b_i + \alpha} e^{-\omega_R} - \frac{\chi^* + b_i}{\chi + b_i + \alpha} \frac{2\chi_I e^{\omega_I}}{2\chi_I - i\alpha} - \frac{\chi^* + b_i + \alpha}{\chi + b_i} \frac{2\chi_I e^{-\omega_I}}{2\chi_I + i\alpha}}{2\cosh(\omega_R) - \frac{2\chi_I e^{\omega_I}}{2\chi_I - i\alpha} - \frac{2\chi_I e^{-\omega_I}}{2\chi_I + i\alpha}} \right) e^{\theta_i + \varphi_i},$$

where

$$e^{\varphi_i} = \frac{\chi + \alpha + b_i}{\chi^* + \alpha + b_i}, \quad \omega_R = \alpha \chi_I t, \quad \omega_I = i\alpha \left[x + \left(\chi_R + \frac{\alpha}{2} \right) t - \frac{1}{2\chi_I} \right],$$

and the parameter $\chi = \chi_R + \chi_I i$ satisfies that

$$1 + \sum_{i=1}^{N} \frac{a_i^2}{(\chi + b_i)(\chi + \alpha + b_i)} = 0,$$

which is the determined equation for the AB solution. Denoting $\chi = \Omega_k - \frac{\mu_k}{2}$, $\alpha = \mu_k$, we find that the pairs (χ,α) and $(\Omega_k - \frac{\mu_k}{2},\mu_k)$ satisfy the same Eq. (8). Namely, the two independent pairs do admit an identical relation. To understand the obtained quantitative relations, we need to make the following expansion. Taking $t \to -\infty$, we obtain the asymptotical expansions

$$q_i = a_i e^{\theta_i}[1 + 2\alpha\chi_I B_i e^{\omega_R} + o(e^{\omega_R})],$$

where

$$B_i = \frac{e^{\omega_I}}{(2\chi_I - i\alpha)(\chi^* + \alpha + b_i)} - \frac{e^{-\omega_I}}{(2\chi_I + i\alpha)(\chi + b_i)}.$$

This is exactly the perturbation assumption in linear stability analysis if the high-order terms are ignored. Thus we answer why the parameters of the AB solution are consistent with MI analysis. Letting $\alpha \to 0$, the fundamental AB solution becomes the fundamental RW solution (2). Naturally, the dispersion relation reduces into Eq. (3) or Eq. (9). In this way, we completely explain why the RW solutions are related with the MI quantitatively.

The number for fundamental RWs in each component can be N at most for N-component coupled NLSE described systems. Furthermore, the explicit number and structure of fundamental RWs can be evaluated by simple MI analysis results. Possibilities to test the theoretical results are also discussed. The results here can be extended to a three-wave resonant system [15,58], scalar NLSE with high-order effects [59–61], and other nonlinear systems [62–68].

ACKNOWLEDGMENTS

We are grateful to Prof. Yan-Jun Chen for his helpful discussions. This work is supported by the National Natural Science Foundation of China (Contracts No. 11401221, No. 11771151, No. 11775176, and No. 11405129).

[1] M. Onorato, S. Residori, U. Bortolozzo, A. Montina, and F. T. Arecchi, Phys. Rep. **528**, 47 (2013).
[2] B. Kibler, J. Fatome, C. Finot *et al.*, Nat. Phys. **6**, 790 (2010).
[3] A. Chabchoub, N. P. Hoffmann, and N. Akhmediev, Phys. Rev. Lett. **106**, 204502 (2011); A. Chabchoub, N. Hoffmann, M. Onorato, and N. Akhmediev, Phys. Rev. X **2**, 011015 (2012).
[4] H. Bailung, S. K. Sharma, and Y. Nakamura, Phys. Rev. Lett. **107**, 255005 (2011).
[5] B. Frisquet, B. Kibler, P. Morin, F. Baronio, M. Conforti, G. Millot, and S. Wabnitz, Sci. Rep. **6**, 20785 (2016).
[6] B. Frisquet, B. Kibler, J. Fatome, P. Morin, F. Baronio, M. Conforti, G. Millot, and S. Wabnitz, Phys. Rev. A **92**, 053854 (2015).
[7] V. Ruban, Y. Kodama, M. Ruderma *et al.*, Europhys. J. Spec. Top. **185**, 5 (2010).
[8] N. Akhmediev and E. Pelinovsky, Europhys. J. Spec. Top. **185**, 1 (2010).
[9] C. Kharif and E. Pelinovsky, Eur. J. Mech. B Fluids **22**, 603 (2003).
[10] E. Pelinovsky and C. Kharif, *Extreme Ocean Waves* (Springer, Berlin, 2008).
[11] Y. V. Bludov, V. V. Konotop, and N. Akhmediev, Europhys. J. Spec. Top. **185**, 169 (2010).
[12] L. C. Zhao and J. Liu, J. Opt. Soc. Am. B **29**, 3119 (2012).
[13] S. H. Chen and L. Y. Song, Phys. Rev. E **87**, 032910 (2013).
[14] L. C. Zhao and J. Liu, Phys. Rev. E **87**, 013201 (2013).
[15] F. Baronio, M. Conforti, A. Degasperis, and S. Lombardo, Phys. Rev. Lett. **111**, 114101 (2013).
[16] S. Chen, X.-M. Cai, P. Grelu, J. M. Soto-Crespo, S. Wabnitz, and F. Baronio, Opt. Express **24**, 5886 (2016).
[17] L. C. Zhao, G. G. Xin, and Z. Y. Yang, Phys. Rev. E **90**, 022918 (2014).
[18] J. S. He, H. R. Zhang, L. H. Wang, K. Porsezian, and A. S. Fokas, Phys. Rev. E **87**, 052914 (2013).
[19] L. M. Ling and L. C. Zhao, Phys. Rev. E **88**, 043201 (2013).
[20] P. Gaillard, Ann. Phys. **355**, 293 (2015); Phys. Rev. E **88**, 042903 (2013); Theor. Math. Phys. **189**, 1440 (2016).
[21] D. J. Kedziora, A. Ankiewicz, and N. Akhmediev, Phys. Rev. E **88**, 013207 (2013).
[22] G. Mu, Z. Qin, and R. Grimshaw, SIAM J. Appl. Math. **75**, 1 (2015).
[23] X. Y. Wen and Z. Yan, Chaos **25**, 123115 (2015).
[24] J. M. Dudley, G. Genty, F. Dias *et al.*, Opt. Express **17**, 21497 (2009).
[25] F. Baronio, M. Conforti, A. Degasperis, S. Lombardo, M. Onorato, and S. Wabnitz, Phys. Rev. Lett. **113**, 034101 (2014).
[26] F. Baronio, S. Chen, P. Grelu, S. Wabnitz, and M. Conforti, Phys. Rev. A **91**, 033804 (2015).
[27] L. C. Zhao and L. Ling, J. Opt. Soc. Am. B **33**, 850 (2016).
[28] G. Biondini and D. Mantzavinos, Phys. Rev. Lett. **116**, 043902 (2016).
[29] V. E. Zakharov and A. A. Gelash, Phys. Rev. Lett. **111**, 054101 (2013).
[30] A. M. Turner, R. Barnett, E. Demler, and A. Vishwanath, Phys. Rev. Lett. **98**, 190404 (2007); F. Zhou and G. W. Semenoff, *ibid.* **97**, 180411 (2006).
[31] L. He and S. Yi, Phys. Rev. A **80**, 033618 (2009); H. Makela and K.-A. Suominen, *ibid.* **75**, 033610 (2007).
[32] A. Mecozzi, C. Antonelli, and M. Shtaif, Opt. Express **20**, 11673 (2012); S. Warm and K. Petermann, *ibid.* **21**, 519 (2013).
[33] B. L. Guo and L. M. Ling, Chin. Phys. Lett. **28**, 110202 (2011).
[34] F. Baronio, A. Degasperis, M. Conforti, and S. Wabnitz, Phys. Rev. Lett. **109**, 044102 (2012).
[35] G. P. Agrawal, *Nonlinear Fiber Optics*, 4th ed. (Academic, San Diego, 2007).
[36] P. G. Kevrekidis, D. Frantzeskakis, and R. Carretero- Gonzalez, *Emergent Nonlinear Phenomena in Bose-Einstein Condensates: Theory and Experiment* (Springer, Berlin, 2009).
[37] Y. Kawaguchi and M. Ueda, Phys. Rep. **520**, 253 (2012).
[38] Z. Yan, Nonlinear Dyn. **79**, 2515 (2015).

[39] L. M. Ling, B. L. Guo, and L. C. Zhao, Phys. Rev. E **89**, 041201(R) (2014); L.-C. Zhao, B. Guo, and L. Ling, J. Math. Phys. **57**, 043508 (2016).
[40] L. Ling, Discrete Contin. Dyn. Syst. Ser. S **9**, 1975 (2016).
[41] J. M. Soto-Crespo, N. Devine, and N. Akhmediev, Phys. Rev. Lett. **116**, 103901 (2016).
[42] M. G. Forest, D. W. McLaughlin, D. J. Muraki, and O. C. Wright, J. Nonlinear Sci. **10**, 291 (2000)
[43] T. Kanna and M. Lakshmanan, Phys. Rev. Lett. **86**, 5043 (2001).
[44] M. G. Forest, S. P. Sheu, and O. C. Wright, Phys. Lett. A **266**, 24 (2000).
[45] T. Xu and B. Tian, J. Phys. A: Math. Theor. **43**, 245205 (2010).
[46] V. B. Matveev and M. A. Salle, *Darboux Transformations and Solitons* (Springer, Berlin, 1991).
[47] C. H. Gu, H. S. Hu, and Z. X. Zhou, *Darboux Transformations in Integrable Systems: Theory and Their Applications to Geometry* (Springer, Berlin, 2006).
[48] L. Ling and L.-C. Zhao, arXiv:1704.00404.
[49] Y. Ohta and J. K. Yang, Proc. R. Soc. A **468**, 1716 (2012).
[50] B. L. Guo, L. M. Ling, and Q. P. Liu, Phys. Rev. E **85**, 026607 (2012).
[51] A. Ankiewicz, N. Devine, and N. Akhmediev, Phys. Lett. A **373**, 3997 (2009).
[52] U. Bandelow and N. Akhmediev, Phys. Lett. A **376**, 1558 (2012).
[53] Y. V. Bludov, R. Driben, V. V. Konotop, and B. A. Malomed, J. Opt. **15**, 064010 (2013).
[54] R. A. Van Gorder, J. Phys. Soc. Jpn. **83**, 054005 (2014).
[55] J. Cuevas-Maraver, P. G. Kevrekidis, D. J. Frantzeskakis, N. I. Karachalios, M. Haragus, and G. James, Phys. Rev. E **96**, 012202 (2017).
[56] G. Yang, L. Li, S. Jia, and D. Mihalache, Rom. Rep. Phys. **65**, 902 (2013).
[57] S. Toenger, G. Genty, F. Dias *et al.*, Sci. Rep. **5**, 10380 (2015).
[58] A. Degasperis, M. Conforti, F. Baronio, and S. Wabnitz, Phys. Rev. Lett. **97**, 093901 (2006).
[59] R. Hirota, J. Math. Phys. **14**, 805 (1973).
[60] N. Sasa and J. Satsuma, J. Phys. Soc. Jpn. **60**, 409 (1991).
[61] X. Y. Wen, Y. Yang, and Z. Yan, Phys. Rev. E **92**, 012917 (2015).
[62] K. Porsezian and K. Nakkeeran, Phys. Rev. Lett. **76**, 3955 (1996); K. Nakkeeran, K. Porsezian, P. S. Sundaram, and A. Mahalingam, *ibid.* **80**, 1425 (1998).
[63] Y. Zhang and W. X. Ma, App. Math. Comp. **256**, 252 (2015).
[64] J. Chen, Y. Chen, B. F. Feng *et al.*, Phys. Lett. A **379**, 1510 (2015).
[65] P. A. Clarkson and E. Dowie, arXiv:1609.00503.
[66] A. Ankiewicz, A. P. Bassom, P. A. Clarkson *et al.*, Stud. Appl. Math. **139**, 104 (2017).
[67] P. Dubard, P. Gaillard, C. Klein *et al.*, Europhys. J. Spec. Top. **185**, 247 (2010).
[68] J. He, S. Xu, K. Porsezian, Y. Cheng, and P. T. Dinda, Phys. Rev. E **93**, 062201 (2016); C. Li, J. He, and K. Porsezian *ibid.* **87**, 012913 (2013).